

Biomechanical behavior of the *Perumytilus purpuratus* shell: symmetry, homogeneity, and remodeling of the mechanical properties

Estefano Muñoz-Moya^a, Claudio M. García-Herrera^{a,*}, Nelson A. Lagos^b, Aldo F. Abarca-Ortega^{a,c}, Antonio G. Checa^d

^aDepartamento de Ingeniería Mecánica, Universidad de Santiago de Chile, Av. Bernardo O'Higgins 3363, Santiago de Chile, Chile

^bCentro de Investigación e Innovación para el cambio climático (CiiCC), Universidad Santo Tomás, Av. Ejército Libertador 146, Santiago de Chile, Chile

^cCenter for Biomedical Technology, Universidad Politécnica de Madrid, 28223 Pozuelo de Alarcón, Spain

^dDepartamento de Estratigrafía y Paleontología, Universidad de Granada, 18071, Granada, España

Abstract

The bivalve mussel *Perumytilus purpuratus* forms dense three-dimensional matrices that constitute a microhabitat for a wide variety of organisms, thus promoting meaningful effects on coastal biodiversity in wave-exposed intertidal habitats, where it is subjected to relevant mechanical stress due to physical forces and durophagous predators. The carbonate shell of mussels protects the soft body parts, and its biomechanical properties are critical for maintaining their integrity and functionality. This work aims to characterize for the first time the shell material of *P. purpuratus* by analyzing its anisotropic biomechanical properties of orthotropic behavior, thus studying three hypotheses, including evaluating the shell's nacreous microstructure's failure characteristics. Firstly, if the biomechanical properties of the left and right shells of the mollusk show symmetrical performance; secondly, if the mechanical properties show a homogeneous behavior along the mollusk shell; thirdly, if the mechanical properties of the shell show remodeling along the ontogeny of the calcium carbonate exoskeleton, i.e., changes in mechanical properties during the aging of the individual. For the mollusk shell's anisotropic characterization, uniaxial compression tests oriented in three orthogonal axes corresponding to the material's orthotropic directions (thickness, longitudinal, and transversal) were performed. The results indicate symmetrical biomechanical performance in the left and right valves. Significant differences were found in the three directions of the shell's mechanical behavior, evidencing the material's anisotropy. No significant differences in mechanical properties were found across the length of the shell, and significant differences were found during ontogeny for one of the orthotropy directions, the thickness direction, suggesting deterioration during material remodeling in mussel growth. SEM analysis suggests that compression testing induces effects of delamination in the mineralogical structure of *P. purpuratus* shells.

Keywords: Bivalves, Biomechanics, Elastic anisotropy, Mechanical properties

¹ **1. Introduction**

² The bivalve mussel *Perumytilus purpuratus* is a common species that inhabit the wave-
³ exposed rocky intertidal of Peru and Chilean coasts [1]. This mussel can form dense
⁴ three-dimensional matrices in the mid-tidal zone, being a dominant competitor of the
⁵ primary substrate [2, 3]. This three-dimensional matrix makes him an essential engineer
⁶ of ecological systems given the increase in species richness registered within *P. purpuratus*
⁷ matrices, which comprise up to 92 different invertebrate taxa [4]. Therefore, this species'
⁸ loss could decrease local biodiversity [5]. Due to this ecological role, many studies have been
⁹ carried out on the effects of predators [6–12] and environmental factors, such as climate
¹⁰ change [13–19], on *P. purpuratus* shells. The strength and functionality of the mollusk shells
¹¹ are essential to confronting natural predators and environmental stress and thus increase
¹² survival opportunities. However, the mechanical properties of the shell of *P. purpuratus*
¹³ have not yet been characterized. Thus, we analyzed the biomechanics of the shells of this
¹⁴ mollusk, evaluating three hypotheses that are not usually corroborated in bivalves, such
¹⁵ as symmetrical mechanical performance between the left and right valves, homogeneity
¹⁶ of mechanical properties across the length of the shell, and remodeling of the mechanical
¹⁷ properties during ontogeny.

¹⁸

¹⁹ The shell of mollusks is a material composed of organic and mineral phases. The compo-
²⁰ sition of the *P. purpuratus* shell is 5% organic matter and 95% inorganic matter in the form
²¹ of aragonite (a crystalline form of calcium carbonate) [20]. In the case of bivalves, the shell
²² microstructure may have various configurations or combinations. These configurations are
²³ categorized into eight types described by Taylor and Layman [21]. The *Mytilidae* *P. pur-*
²⁴ *purpuratus* has a nacreous sheet structure [22, 23]. Nacre has a laminar bricks-and-mortar-like
²⁵ structure [24], in which pseudohexagonal tablets arrange into lamellae. The different lamel-
²⁶ lae are glued with soft organic membranes, called interlamellar membranes [25–27]. Nacre
²⁷ is only present in the molluscan classes of gastropods, bivalves and monoplacophorans; and
²⁸ has a complex hierarchical architecture that encompasses multiple length scales from the
²⁹ nanoscale to the macro-scale [25, 28–31].

³⁰

³¹ In biomechanics, the growth process also includes a process called "remodeling" of the
³² material. This process involves changes in material properties. These changes, which often
³³ are adaptive, may be brought about by alterations in modulus, internal structure, strength,
³⁴ or density [32]. Several studies have focused on the mechanics of the nacreous material of
³⁵ bivalves, in which tensile, compression, shear, indentation, bending, and scratching tests
³⁶ have been performed [24, 33], including fracture analysis of the material [34–39]. However,
³⁷ rarely studies have focused on the potential symmetry of the left and right valves, the ho-
³⁸ mogeneity along the shell or ontogenetic effects on the mechanical properties, and specifically
³⁹ in *P. purpuratus*. Meyers et al. has carried out tensile and compression tests in nacreous

*Corresponding author.

Email address: claudio.garcia@usach.cl (Claudio M. García-Herrera)

40 material structures without specifying which valve was used [27]. Mohanty et al. reported
41 on the nanomechanical behavior of nacre (from *Haliotis rufescens* shell) and showed that
42 aragonite platelets have a viscoelastic behavior when organic material is present due to their
43 wet state [40]. The research results by Bezares et al. indicated that under the presence of
44 moisture, the hardness was much lower than the dry state, producing plastic deformation at
45 the edges, indicating anisotropic behavior [41]. Therefore, considering the great importance
46 of the mussel *P. purpuratus* and the lack of studies regarding the symmetry, homogeneity,
47 and remodeling of both shells of bivalve mollusks, we contribute to the understanding of
48 the biomechanical behavior of this type of animals.

49 A wide variety of research related to the mechanical properties and strength of bivalve
50 shells has been carried out to observe adverse effects produced by the environment, such as
51 climate change or predators. However, these do not differentiate the mechanical properties
52 between left and right valves, homogeneity along the shell, or remodeling during mollusk
53 growth. Instead, the same mechanical properties have been assumed in many studies. The
54 research by Immel et al. showed that the shell of the zebra mussel *Dreissena polymorpha*
55 selectively concentrates some heavy metals, in particular uranium, which predisposes the
56 mollusk to local bioremediation of this pollutant; using the left and right shell indistinctly
57 to carry out the microstructural study [42]. Mackenzie et al. evaluated the effects of acid-
58 ification (ambient pH -0.4 pH units) and warming (ambient temperature +4°C) on the
59 strength of *Mytilus edulis* bivalve shells when fed for a limited period (4-6 h day-1). In
60 this study, the individual values of load and extension were considered the mean of each
61 mussel's two valves [43]. Yang et al. studied the structure and mechanical behavior of the
62 bivalve *Saxidomus purpuratus* shell. In this research compression tests, were performed in
63 three different directions of the material, but it is not specified which of the two valves
64 was used for the experiment [44]. Manríquez et al. observed that the predator *Concholepas*
65 *concholepas* attacks the left and right valves of the bivalve mollusk *Perumytilus purpuratus*
66 (study species) indistinctly, which could suggest a symmetry in the mechanical properties
67 of both shells [10]. In Jiao et al.'s research, the mechanical behavior of pearl and nacre with
68 spherical and flat laminations was studied and compared with that of geological aragonite,
69 obtaining the mechanical properties of the bivalve *Sinanodonta woodiana*, although without
70 specifying which valve was used [45]. Fitzer et al. evaluated the fracture resistance of
71 *Mytilus edulis* shells under the effects of climate change; the study considered the average
72 of both shells with no differences between them; also, the sector of the shell analyzed is
73 not specified [46]. However, the question remains open whether the left and right shells
74 have the same mechanical properties, either in the thickness (normal to the surface of the
75 valve), longitudinal (growth directions, and parallel to ribs of the shell), or transversal
76 (perpendicular to the shell ribs) direction, considering that the mechanical behavior of the
77 material is anisotropic.

78 This work aims to characterize the anisotropic biomechanical behavior of *Perumytilus*
79 *purpuratus* shells at the macro level. It is proposed to evaluate differences in the material's
80 mechanical properties between the left and right valve, along the shell, or if the individual's

83 shell sizes affect such mechanical properties along the ontogeny. This will allow complement
 84 existing studies justifying the symmetry of both shells, the sector from which the sample is
 85 extracted, the age of the mollusk studied and will allow performing different analyses to each
 86 of the two valves for different studies, in which the biomechanical characteristics of the mussel
 87 have not been evaluated. For this purpose, uniaxial compression tests have been performed
 88 in three directions of the material corresponding to orthotropic behavior, implementing
 89 an anisotropic linear elastic model. The failure characteristics of the compressed samples
 90 observed with a scanning electron microscope (SEM) and the magnitudes of the mechanical
 91 properties were compared with existing literature.

92 2. Materials and methods

93 2.1. Sample collection

94 In July 2019, individuals of *P. purpuratus* were randomly collected from the intertidal
 95 habitats of the coastal area of Huasco ($28^{\circ}30'S$; $71^{\circ}15'W$), Chile. In the laboratory, indi-
 96 viduals were characterized in length and weight (Table 1), then soft tissues were separated
 97 from the shell material, which was dried at room temperature, and left and right valves were
 98 processed separately. The length, width, height, and thickness of the right shell (figure 1),
 99 as defined by Manríquez et al. [10], were measured with a digital Vernier Calliper (Mitutoyo
 100 ± 0.01 [mm]), the weights of the left and right valves were measured in a analytical balance
 101 (SHIMADZU AUX120 ± 0.0001 [g]), as shown in Table 1. All animals received humane
 102 care in compliance with the principles of laboratory animal care, the Ethics Committees
 103 approved all animal care and experimental procedures of the Universidad Santo Tomás and
 104 the Universidad de Santiago de Chile (IE N° 0146). They were conducted according to the
 105 Guide for the Care and Use of Laboratory Animals published by the US National Institutes
 106 of Health (NIH Publication No. 85–23, revised 1996).

Table 1: Mean value and the standard error of the mean (\pm SEM): length, height, width, and thickness of the right shell, left valve weight, right valve weight.

Group	Length [mm]	Height [mm]	Width [mm]	Thickness [mm]	Left valve weight [g]	Right valve weight [g]
1	14,42 \pm 0,30	6,55 \pm 0,14	7,67 \pm 0,40	0,40 \pm 0,03	0,15 \pm 0,01	0,15 \pm 0,01
2	19,92 \pm 0,44	10,55 \pm 0,65	10,70 \pm 0,44	0,47 \pm 0,05	0,37 \pm 0,03	0,38 \pm 0,02
3	26,18 \pm 0,64	11,77 \pm 0,60	14,15 \pm 0,80	0,59 \pm 0,06	0,83 \pm 0,11	0,82 \pm 0,11
4	32,44 \pm 1,30	15,13 \pm 0,51	14,96 \pm 0,23	0,79 \pm 0,03	1,57 \pm 0,15	1,60 \pm 0,21
5	37,55 \pm 1,61	18,46 \pm 0,60	16,76 \pm 0,32	0,72 \pm 0,03	2,71 \pm 0,02	2,77 \pm 0,08

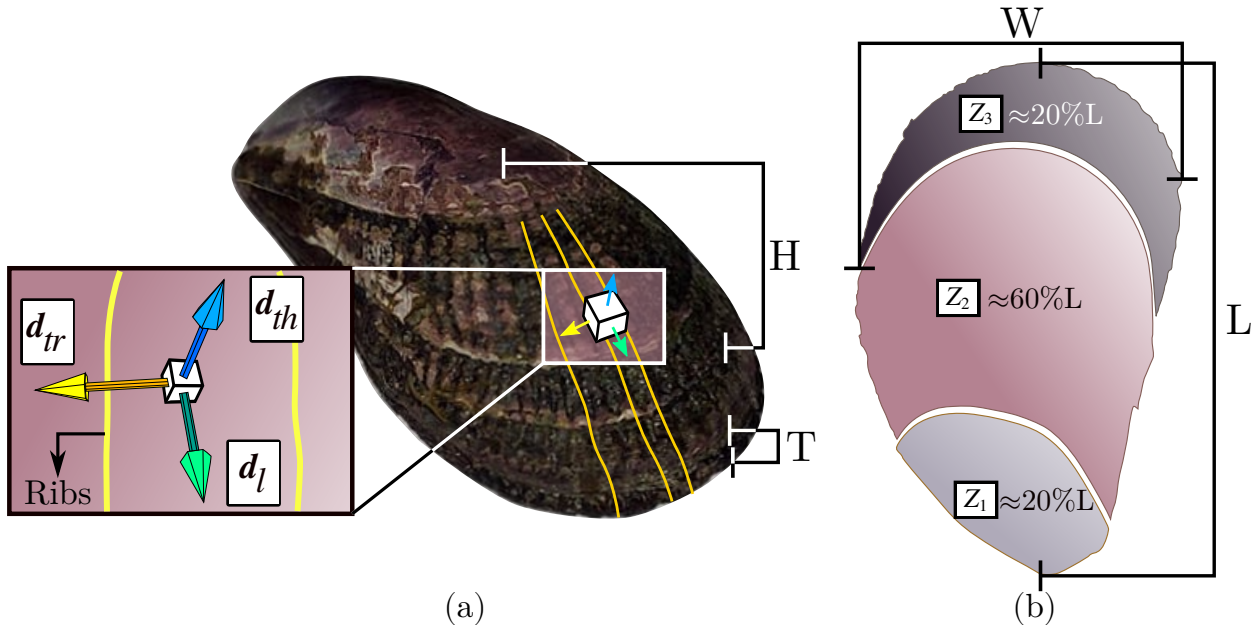


Figure 1: L : Length, H : Height, W : Width, T : Thickness. (a) Orthotropic directions of *P. purpuratus* shell material behavior: Thickness direction (\mathbf{d}_{th}), Longitudinal direction (\mathbf{d}_l) and Transversal direction (\mathbf{d}_{tr}), (b) Zones in which the shell was divided, Zone 1 (Z_1), Zone 2 (Z_2) and Zone 3 (Z_3). The respective percentage of the length is presented for each zone.

107 In this study, 15 mussels were separated into five groups that correspond to the age/size
 108 category from the shell's length, representing their juvenile stage until the mollusk reaches
 109 maturity [2, 18, 47, 48]. In order to observe differences in mechanical properties as the shell
 110 grows, the valves were divided into 3 zones (Z_1 , Z_2 , and Z_3) along its length (figure 1b).
 111 Z_3 is located at the shell margin (posterior), Z_1 corresponds to the sector closest to the
 112 umbo (anterior), and Z_2 is the sector between Z_1 and Z_3 . Therefore, each mollusk has two
 113 valves, left and right, and from each shell sections, three samples (figure 2a) were extracted
 114 to be compressed in the three directions of the material's mechanical behavior (figure 1a):
 115 Thickness direction (\mathbf{d}_{th}), which is normal to the surface of the shell. Longitudinal direction
 116 (\mathbf{d}_l), according to the growth direction, and parallel to the ribs of the shell. Transversal
 117 direction (\mathbf{d}_{tr}), perpendicular to the shell ribs. Directions already evaluated previously in
 118 other bivalves under compression tests [24, 44].
 119

120 2.2. Uniaxial compression test

121 Uniaxial compression tests were performed on an Instron 3342 universal testing machine.
 122 This test consists of compressing a prismatic sample of the shell material with exposed
 123 nacreous layer cross-section (NC), whose orientation coincides with the orthotropic directions
 124 of the material (figure 2a).

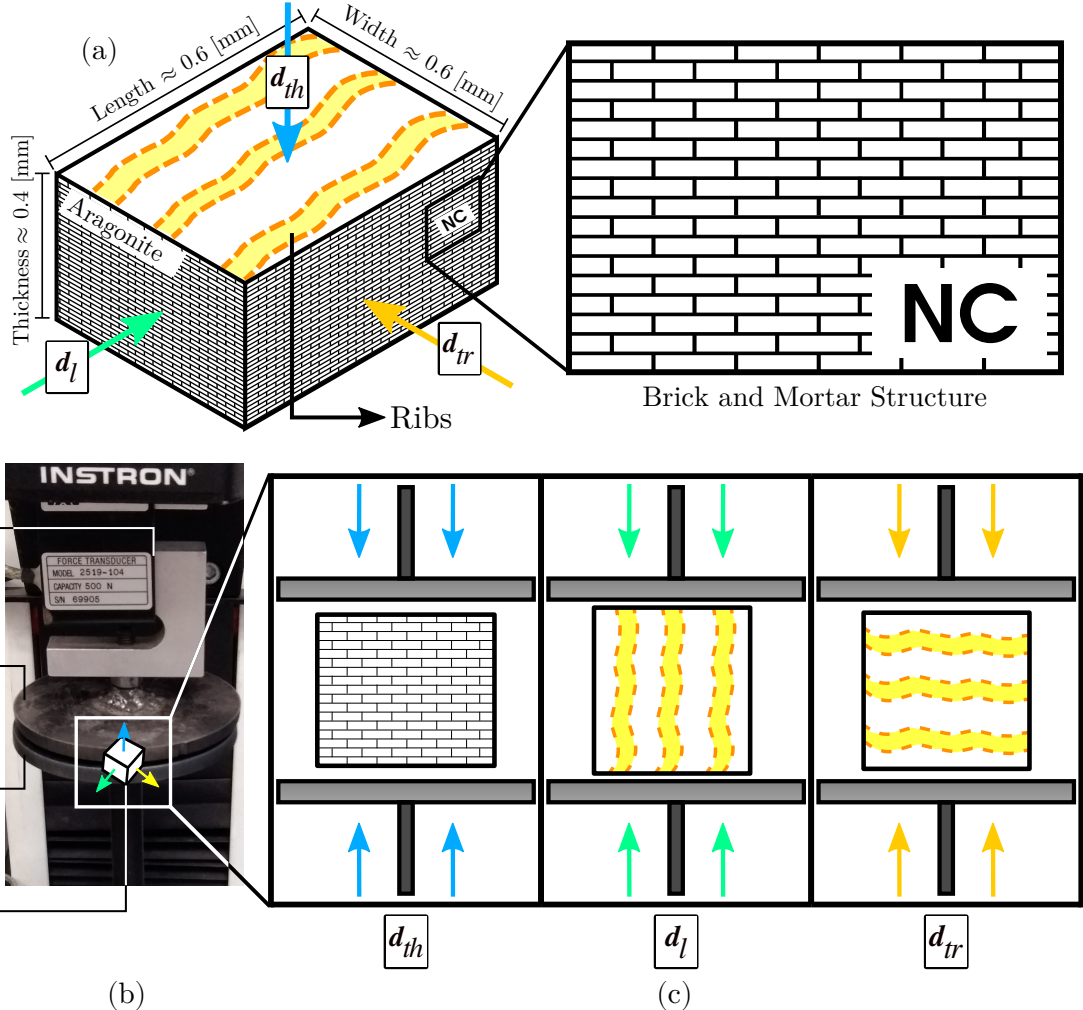


Figure 2: Uniaxial compression test assembly. (a) Orthotropic directions of the nacreous material (bricks-and-mortar structure) represented in the sample used in uniaxial compression test. NC: nacreous layer cross-section, (b) A: Load cell, B: Mobile top plate, C: Fixed bottom plate, D: Sample, (c) Arrangement of the samples according to the direction of compression.

The test was performed using dry shells and applying a compression load (figure 2b), with a constant displacement speed of 0.05 [mm/min], in the three orientations described above, as shown in figure 2c. The reaction force from the mobile plate's imposed displacement was recorded by the load cell (Instron: 2519 series static load cells 500 [N]), as shown in figure 2b. Thus, a total of 270 compression tests were performed.

After the test, load cell force and displacement data (F and d) were acquired. The stress-strain curve (σ - ε) was calculated as follows: $\sigma = F/A_0$ and $\varepsilon = \Delta l/l_0$, where A_0 is the initial cross-sectional area of the sample, normal to the loading direction (d_{th} , d_l , and d_{tr}), l_0 is the initial length of the sample, and Δl is the length variation of the sample during the test. The data allowed us to know its mechanical properties considering a linear orthotropic behavior: elastic modulus (E), maximum stress (σ_{max}), and maximum strain (ε_{max}).

137 **2.3. Statistical methods**

138 To evaluate the differences of the elastic modulus, maximum stress, and maximum strain
139 in the shell of *P. purpuratus*, we use an Analysis of Covariance (ANCOVA) regarding the
140 shell thickness of each individual as a covariate. These mechanical properties were compared
141 between valves (left and right), shell age/size (groups 1 to 5, Table 1), and three zones
142 (Z_1 , Z_2 and Z_3) of each valve (figure 1b), considering these factors as fixed. Tukey's test
143 was performed to evaluate which individual factor levels generated significant differences
144 between the main factors. ANCOVA assumptions were evaluated using the residues of the
145 full model. The analysis was implemented using GLM (general linear model). Both the
146 residue graph and the variance heterogeneity test showed no significant deviations.

147
148 In each analysis, the three mechanical properties (E , σ_{max} , and ε_{max}) of each of the three
149 orthotropic directions of the material (d_{th} , d_l , and d_{tr}) were compared separately to test
150 for differences. The first hypothesis, the symmetry of the mechanical behavior between the
151 left and right valves, the age/size groups were studied separately to avoid the mechanical
152 properties remodeling at different ages of the mollusk. Three samples per shell (left and
153 right) were used without distinction of zones; thus, the number of samples corresponds to
154 nine (n=9). The second hypothesis, the homogeneity of mechanical properties along the
155 shell, each age/size group was analyzed separately. The comparison was made by studying
156 each zone's mechanical properties (without differentiation between left and right valves), so
157 a total of six samples were used for the analysis (n=6). The third hypothesis, the remodeling
158 of mechanical properties during mollusk aging, was compared between the different age/size
159 groups, in which there was no distinction between the three zones and between left and right
160 valves, so the number of samples analyzed was 18 per group (n=18).

161 **2.4. Scanning Electron Microscopy (SEM)**

162 Scanning Electron Microscopy (SEM) were performed on the shell samples used in the
163 uniaxial compression tests, specifically on those compressed in the longitudinal and transver-
164 sal directions (figure 3). The samples were analysed on the surfaces into which the samples
165 were divided (figure 3b), the nacreous layer surface (NS), and on their thickness (figure 3c),
166 the nacreous layer cross-section (NC).

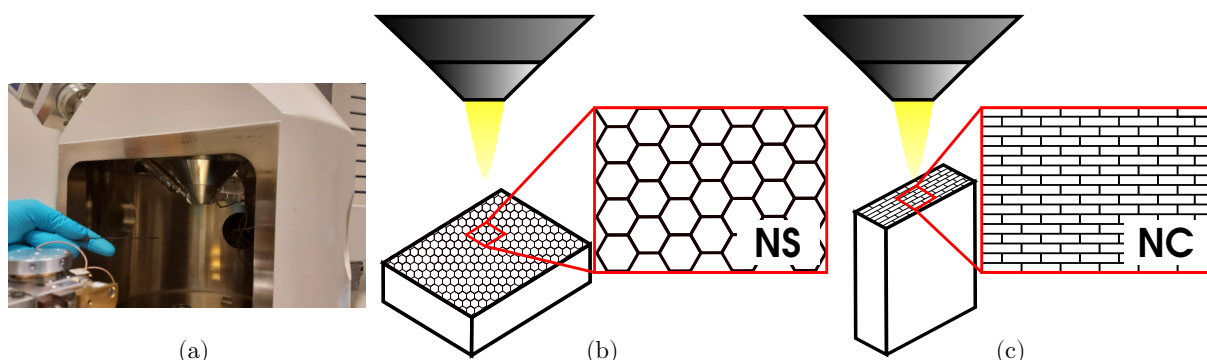


Figure 3: (a) Scanning electron microscope (SEM), model ZEISS EVO 10 SEM, (b) Arrangement of samples for nacreous layer surface (NS), (c) Arrangement of samples for nacreous layer cross-section (NC).

167 SEM observations of the shell compressed samples were performed perpendicular to the
 168 delamination surface (figure 3b), and the other sample halves were used for imaging of
 169 thickness (figure 3c). Subsequently, a gold layer of approximately 30 [nm] thickness was
 170 applied using the Cressington 108 Auto Sputter Coater equipment. The applied gold layer
 171 is known behavior, and its main bands are located at 2.1 [KeV] and 9.7 [KeV]. Finally, the
 172 microscopic examination was performed in a Zeiss EVO MA 10 scanning electron microscope
 173 at 20 [kV] (figure 3a).

174

175 3. Results and discussion

176 3.1. Uniaxial Compression Test

177 The linear regression results corroborate the linear elastic behavior, and it is also ob-
 178 served that the shell material of *P. purpuratus* is brittle, i.e., without a plastic zone, so the
 179 curve only represents the elastic zone in the stress-strain curve. The regression lines with
 180 their respective confidence interval for each age/size group can be seen in figure 4; they
 181 show an apparent symmetry of the mechanical properties between the left and right valves
 182 for all age/size groups, and a decrease or deterioration in the thickness direction's mechan-
 183 ical properties as the mollusk ages, both in maximum stress and maximum strain during
 184 the ontogeny. The other directions do not show an observable deterioration in mechanical
 185 properties. The mechanical properties for each group of shell age/size and the compression
 186 directions can be seen in Table 2.

Table 2: Mean value and the standard error of the mean (\pm SEM): elastic modulus (E), maximum stress (σ_{max}) and maximum strain (ε_{max}) for each age/size group and orthotropy direction of the shell material, the thickness (d_{th}), longitudinal (d_l), and transversal (d_{tr}) directions.

Group	Direction	E [MPa]		σ_{max} [MPa]		ε_{max}	
1	d_{th}	495.5	\pm	57.5	178.5	\pm	38.9
	d_l	1937.5	\pm	173.2	109.4	\pm	13.1
	d_{tr}	1643.3	\pm	154.6	103.8	\pm	16.7
2	d_{th}	591.8	\pm	50.1	175.9	\pm	21.7
	d_l	1878.4	\pm	126.6	122.1	\pm	11.2
	d_{tr}	1693.5	\pm	157.8	100.2	\pm	12.5
3	d_{th}	594.8	\pm	46.2	129.8	\pm	19.7
	d_l	1817.9	\pm	139.6	131.3	\pm	13.2
	d_{tr}	1604.1	\pm	126.5	117.1	\pm	11.7
4	d_{th}	596.6	\pm	48.9	137.1	\pm	16.6
	d_l	1631.9	\pm	102.3	131.1	\pm	15.1
	d_{tr}	1545.5	\pm	108.6	122.0	\pm	15.2
5	d_{th}	517.4	\pm	36.5	93.8	\pm	9.8
	d_l	1614.4	\pm	121.1	114.9	\pm	12.3
	d_{tr}	1697.2	\pm	156.7	104.6	\pm	12.9

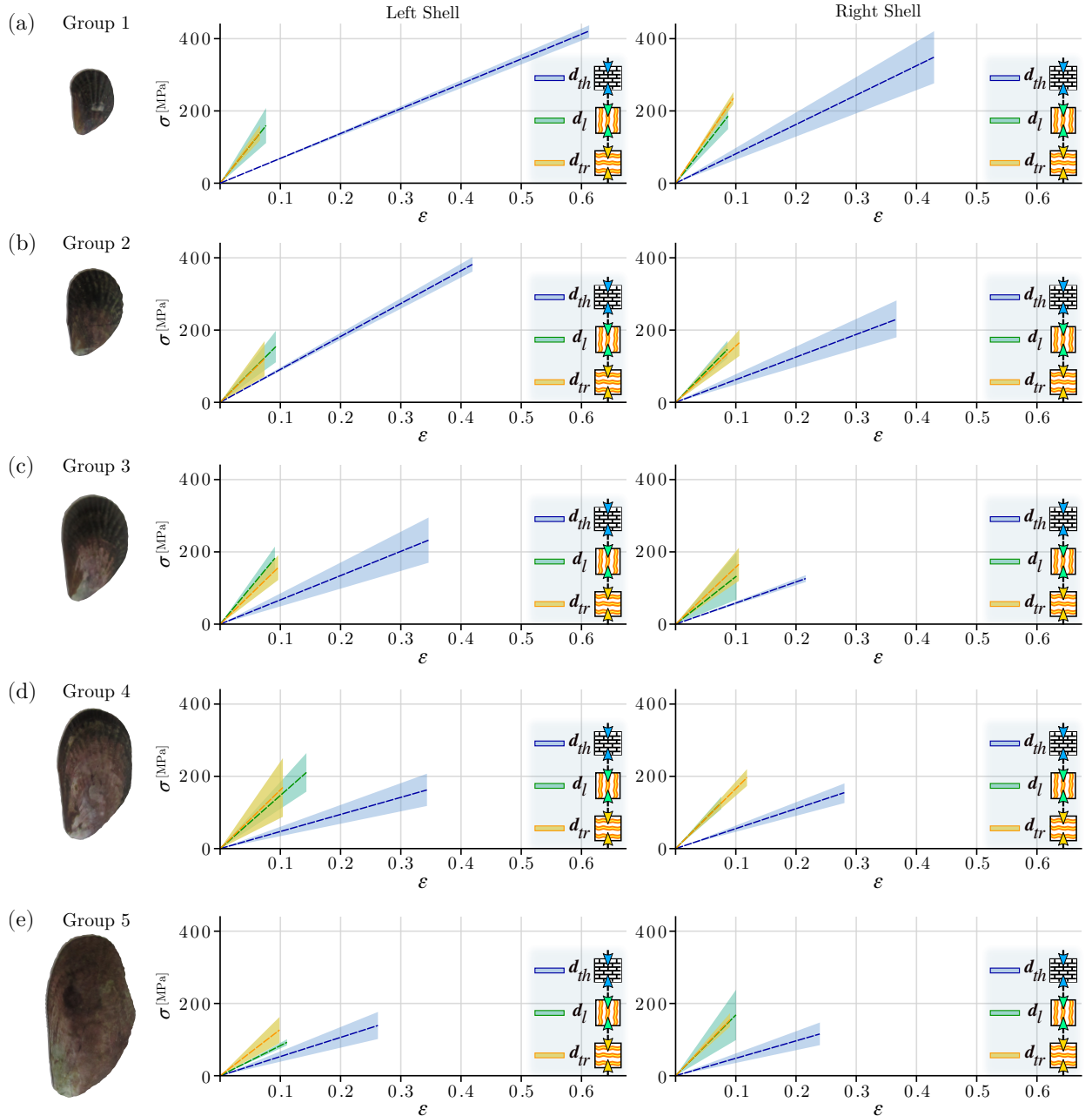


Figure 4: Standard deviation (SD) of the stress-strain curve (σ - ϵ) of the five age/size groups (with a representation of each group's right valve) for the left and right shells in their respective orthotropic directions of the material; thickness (d_{th}), longitudinal (d_l) and transversal (d_{tr}) direction. (a) group 1, (b) group 2, (c) group 3, (d) group 4, (e) group 5.

187 3.1.1. Statistical results

188 The results of the ANCOVA analysis (Table 3) indicated that the elastic modulus,
 189 maximum stress, and maximum strain showed no significant differences when comparing
 190 both shell valves (left and right) and the three shell zones of *P. purpuratus*. The factors'

191 shell age/size and direction of compression showed significant differences between levels of
 192 each factor. Therefore, there was a significant difference between at least two directions of
 193 orthotropy of the material. Still, there were no differences between the three zones and the
 194 left and right valves of the mechanical properties.

195

Table 3: Results of ANCOVA analysis for elastic modulus (E), maximum stress (σ_{max}), and maximum strain (ε_{max}). The shell thickness (T) [mm] of each individual was used as a covariate. Five size ranges (S), the left and right valves (V), the three shell zones (Z), and three compression directions (d) were considered. DF = Degrees of Freedom; SS = Sum of Squares; F = F-statistic; p = p -value.

Variation factors	Elastic Modulus (E)				Maximum stress (σ_{max})				Maximum strain (ε_{max})			
	DF	SS	F	p	DF	SS	F	p	DF	SS	F	p
Thickness (T)	1, 179	8482661	36.85	<0.001	1, 179	116753	21.82	<0.001	1, 179	0.010349	1.69	0.195
Size (S)	4, 179	2231018	9.69	<0.001	4, 179	35405	6.62	<0.001	4, 179	0.012374	2.03	0.093
Left-right valve (V)	1, 179	392566	1.71	0.193	1, 179	11361	2.12	0.147	1, 179	0.015988	2.62	0.107
Zone (Z)	2, 179	429319	1.87	0.158	2, 179	1069	0.2	0.819	2, 179	0.006161	1.01	0.36
Direction (d)	2, 179	39192966	170.27	<0.001	2, 179	25728	4.81	0.009	2, 179	0.940001	153.96	0.001
$S \times V$	4, 179	182587	0.79	0.531	4, 179	2473	0.46	0.763	4, 179	0.003177	0.52	0.721
$S \times Z$	8, 179	109154	0.47	0.873	8, 179	8699	1.63	0.120	8, 179	0.009423	1.54	0.145
$S \times d$	8, 179	183583	0.8	0.605	8, 179	8992	1.68	0.106	8, 179	0.020345	3.33	0.001
$V \times Z$	2, 179	118832	0.52	0.598	2, 179	2086	0.39	0.678	2, 179	0.003939	0.65	0.526
$V \times d$	2, 179	71727	0.31	0.733	2, 179	11000	2.06	0.131	2, 179	0.019201	3.14	0.045
$Z \times d$	4, 179	351214	1.53	0.197	4, 179	9821	1.84	0.124	4, 179	0.00546	0.89	0.469
$S \times V \times Z$	8, 179	22719	0.1	0.999	8, 179	2460	0.46	0.883	8, 179	0.003062	0.5	0.854
$S \times V \times d$	8, 179	91868	0.4	0.920	8, 179	4409	0.82	0.583	8, 179	0.009067	1.49	0.165
$S \times Z \times d$	16, 179	205562	0.89	0.578	16, 179	4794	0.9	0.575	16, 179	0.00628	1.03	0.429
$V \times Z \times d$	4, 179	245962	1.07	0.374	4, 179	5454	1.02	0.399	4, 179	0.00171	0.28	0.891
$S \times V \times Z \times d$	16, 179	73345	0.32	0.995	16, 179	4585	0.86	0.620	16, 179	0.003485	0.57	0.903

196 After ANCOVA's analysis, Tukey's tests were performed, which revealed differences
 197 between the mechanical properties (E , σ_{max} , and ε_{max}) in the thickness direction and the
 198 longitudinal and transversal directions ($p < 0.05$). There were no significant differences
 199 between the longitudinal and transversal directions. *P. purpuratus* sizes revealed significant
 200 differences in mechanical properties in the three orthotropic directions for the different sizes
 201 ($p < 0.05$), i.e., decreasing the magnitude of the mechanical properties until size 5 (figure
 202 4). Therefore, in general, the three mechanical properties of each direction present a greater
 203 magnitude in the first three sizes, to decrease and be constant in sizes 4 and 5 subsequently.
 204

205 Also, it is observed that the thickness direction has mechanical properties that give it
 206 the quality of greater elasticity in the juvenile stages of the individual, both in the maximum
 207 stress and maximum strain. Nevertheless, the maximum stress decreases at large sizes, and
 208 its values reach lower magnitudes than the other directions in the same age. Therefore, the
 209 material becomes brittle with shell size (age), especially in the thickness direction.
 210

211 Considering the remodeling in the biomechanics of the shell during ontogeny, it can be
 212 observed in Table 1 that the thickness direction varies its mechanical properties from the
 213 youngest to the oldest individuals (groups 1 to 5), as follows: $\sigma_{max} = 178 - 93$ [MPa] and
 214 $\varepsilon_{max} = 0.3 - 0.18$. However, the elastic modulus does not present such notable variations;
 215 the results show that the magnitudes range from 495 to 596 [MPa]. The other directions

216 (\mathbf{d}_l and \mathbf{d}_{tr}) show no difference in the mechanical properties between them, in addition to
217 not varying at great extend during ontogeny, the average mechanical properties for both
218 are as follows: $\sigma_{max} = 126$ [MPa] and $\varepsilon_{max} = 0.13$; the elastic modulus varies between the
219 different ages (groups 1 to 5), in the form $E = 1790 - 1655$ [MPa].
220

221 There are many studies are related to the mechanical properties of mollusk shells ob-
222 tained in quasi-static compression tests for shell materials with nacreous microstructure in
223 a dry state, specifically in the gastropod family, such as *Haliotis rufescens*, studied in the
224 work of [Menig et al.](#) [49] and compiled (together with other works of nacreous material),
225 in the review made by [Sun and Bhushan](#) [24]. The values reported corresponding to the
226 mechanical properties in the thickness direction and the longitudinal and transversal direc-
227 tions, the latter two without distinction. For the thickness direction, the elastic modulus
228 values range from 70 to 114 [MPa], and the values for the maximum stress range from 250 to
229 540 [MPa]. The longitudinal and transversal directions present only maximum stress values,
230 being approximately 235 [MPa].

231 *3.1.2. Failure characteristic*

232 The sample used (figure 2a) reaches the point of the fracture without plastic deforma-
233 tion. However, when the failure strength of the samples was reached, an interesting effect
234 is observed. The fracture of the samples differs depending on the direction in which it is
235 compressed. The thickness direction does present a tortuous fracture of the sample, usually
236 fragmented into many pieces during the test; it is pulverized or broken, whereas the longitu-
237 dinal and transversal directions present a particular pattern observed in all cases, as shown
238 in figure 5. Out of a total of 180 samples compressed in the directions mentioned above (\mathbf{d}_l
239 and \mathbf{d}_{tr}), 95% of them failed due to delamination at maximum stress, an effect described by
240 many authors called tortuosity [23, 25, 49–53], one of the toughening mechanisms proposed
241 by [Sarikaya](#) [50]. In their respective studies, the authors reported that the samples in the
242 three directions defined in this work fail by this type of fracture, which they observed using
243 microscopes, concluding that the cracks follow the aragonite tiles pattern, a path known as
244 tortuous fracture path (TFP).
245

246 Figure 5a, shows the failure of the sample when a load is applied in the thickness direction,
247 a TFP during the crack propagation. Fracture in this direction for nacreous materials
248 has been observed and reported mostly in flexure tests and fracture analysis [24, 36, 38,
249 54], whose crack propagation advances between the aragonite platelets in the thickness
250 direction. The study conducted by [Menig et al.](#) reports the type of failure observed in the
251 *P. purpuratus* mussel, bending, shear, and compression tests were performed on *Haliotis*
252 *rufescens* (abalone) shells across the same directions used in our study. These authors
253 observed that the thickness direction's failure suffered a cracks deflection by organic layers,
254 following the platelets path; delamination and micro buckling under compression occurred
255 in the other directions [49].

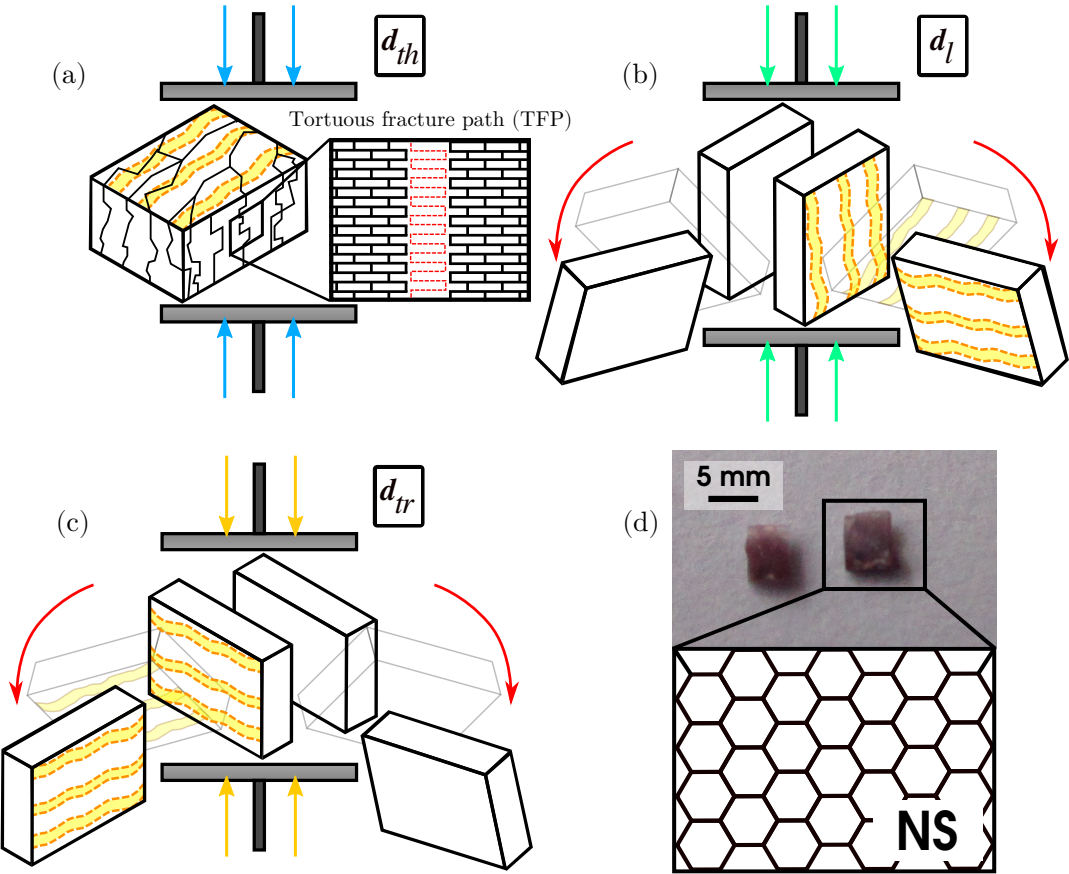


Figure 5: Failure characteristic of the sample at the end of the uniaxial compression test in the thickness (d_{th}), longitudinal (d_l), and transversal (d_{tr}) directions. (a) Fractured sample by failure with an apparently tortuous fracture at the end of the test in the thickness direction (d_{th}), (b) Fractured sample by delamination at the end of the compression test in the longitudinal direction (d_l), (c) Fractured sample by delamination at the end of the compression test in the transversal direction (d_{tr}), (d) Photograph of fractured sample and its microstructure after applying compression in the longitudinal (d_l) and transversal (d_{tr}) direction. NS: nacreous layer surface.

Extrapolating this type of failure to other materials, it is possible to find a vast literature on a non-organic brick-and-mortar structure, such as masonry [55–59]. The investigations of these structures include mechanical tests of uniaxial normal forces to its surface, both in compression and tension, shear tests, bending, and fracture analysis, in which the failure by compression in which a load is applied in the same directions of this study (in the thickness direction and exerting the load force in the longitudinal or transversal direction, without distinction) causes a failure similar to the samples of nacreous structures.

A highly tortuous fracture surface of the nacre is visible on SEM imaging (figure 6a), which is seen in the same direction as the applied force (F) on samples compressed in the longitudinal and transversal directions. The microlayers consist of hexagonal tiles shown in figure 6b, and the analysis of the fracture surface at higher magnification reveals a tortuous fracture path (figure 6d), which is similar to the results reported by Menig et al. [49].

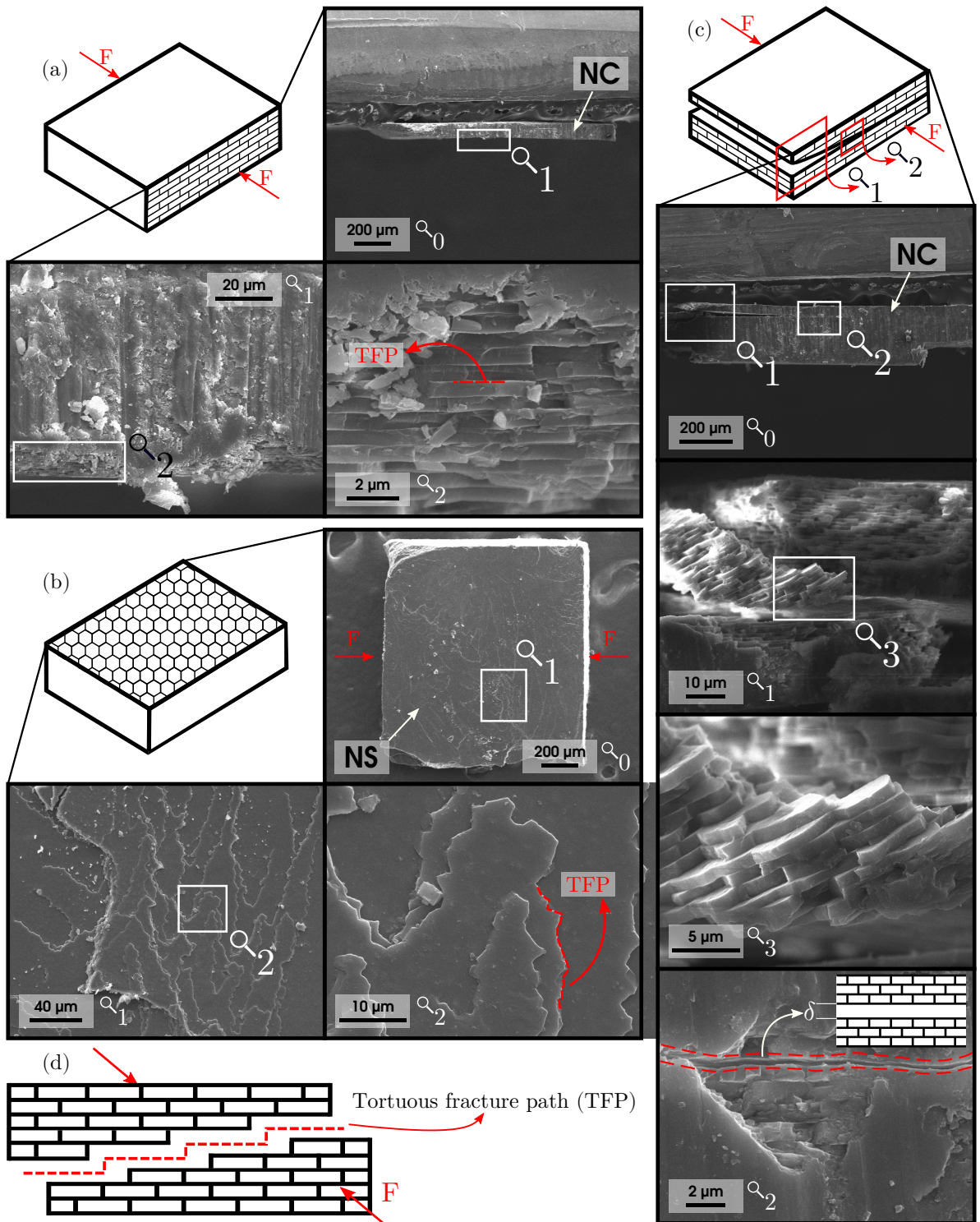


Figure 6: SEM images of the sample at the end of the compression test in the longitudinal (\mathbf{d}_l) and transversal (\mathbf{d}_{tr}) directions. (a) Imaging on the nacreous layer surface (NS), (b) imaging on the layer cross-section (NC), (c) sample with incomplete delamination, whose fracture origin has an aragonite "bricks" separation of δ , (d) tortuous fracture path (TFP). F: direction of the applied force

269 The images reveal that the fracture path's direction is perpendicular to the force applied
270 in compression (F). This can be corroborated in figure 6c, which is a sample that suffered
271 delamination in more than one plane, and one was incomplete, so it is possible to observe
272 the fracture path. At the origin, there is a separation of the tiles at a distance δ (figure
273 6c.2), and at the end of the fracture, there is a separation of the aragonite platelets (fig-
274 ure 6c.1), including a tilted column as a result of the detachment of the material (figure 6c.3).

275
276 Finally, another aspect to consider of the microstructure of *P. purpuratus* corresponds
277 to the thickness of the aragonite tiles, which is approximately 0.6 [μm] (measured using the
278 SEM images). This value differs from the thickness of the tiles reported by Menig et al.
279 and Meyers et al. in the nacreous microstructure of *Haliotis rufescens* (~ 0.5 [μm]) [49, 60].
280 However, the thickness of nacre tablets regularly varies within the same individual, so it does
281 not necessarily play a fundamental role in the difference between the mechanical properties
282 of the two species.

283 4. Conclusions

284 This research was devoted to characterizing the biomechanical behavior of the *Perumytilus purpuratus* shell through performing quasi-static compression tests. The results
285 indicated a similar performance in the mechanical properties of the longitudinal and
286 transversal directions, although both are statistically different to the thickness direction,
287 evidencing the orthotropic behavior of the nacreous material. The results also evidenced a
288 symmetrical behaviors in elastic modulus, maximum stress, and maximum strain of both
289 valves, and homogeneity in the mechanical behavior across the shell zones. However, the
290 elastic modulus recorded in the three orthotropic directions of the material was negatively
291 affected as the mollusk increases in size/age, although the thickness direction is the one
292 that undergoes more changes, also decreasing the maximum stress and maximum strain to a
293 great extent during the ontogeny. Besides, SEM images of the samples' microstructure used
294 in the compression test were obtained to study the material's failure characteristics. These
295 presented a similar failure mode to the samples reported in studies of nacreous material, a
296 tortuous failure, including delamination in the compressed samples in the longitudinal and
297 transversal directions.

298
299 Considering these results, for future studies that require knowing the mechanical prop-
300 erties of the mollusk *P. purpuratus*, it is possible to obtain them without distinction of both
301 shells or along the shell. However, it is necessary to differentiate between the orthotropic
302 directions of the material and the age of the mollusk, mainly if the mechanical properties are
303 evaluated in the thickness direction, considering that it is the one that undergoes the most
304 significant changes. This research could also be considered to analyze the biomechanics of
305 the shell of different bivalves whose microstructure is nacreous and thus define the sym-
306 metry, homogeneity, and remodeling of the mechanical properties from the studied mollusks.

309 It is interesting to note the structural similarity of the shell material to human structures
310 on the failure characteristic, as it is between the nacreous material and masonry. So this
311 information is valuable in studies of biomimetic materials and structures. Besides, the
312 material's failure mode under compression is of great help in the biological understanding
313 between prey-predator or its relationship with the environment. Therefore, it is necessary
314 to generate new studies that experiment with the stress concentrations necessary for the
315 material's delamination and the evolutionary role for the material to behave in this way.

316 **Acknowledgements**

317 The supports provided by the PIA ANILLOS ACT project No. 172037 of the Chilean
318 Council for Research and Technology (ANID - Ex CONICYT), and the Projects CGL2017-
319 85118-P of the Spanish Ministerio de Ciencia e Innovación, and the Research Group
320 RNM363 of the Junta de Andalucía. In addition, we thank the support provided by DICYT
321 from the Universidad de Santiago de Chile and by ANID PFCHA/DOCTORADO BECAS
322 CHILE/2019 – CEL00011051.

323 **CRediT authorship contribution statement**

324 **Estefano Muñoz-Moya:** Conceptualization, Methodology, Software, Validation, Formal
325 analysis, Investigation, Data Curation, Writing - Original Draft, Writing - Review &
326 Editing, Visualization.

327 **Claudio M. García-Herrera:** Conceptualization, Methodology, Formal analysis, Resources,
328 Writing - Original Draft, Writing - Review & Editing, Visualization, Supervision.

329 **Nelson A. Lagos:** Conceptualization, Methodology, Formal analysis, Resources, Writing -
330 Review & Editing, Visualization, Supervision, Funding acquisition, Project administration.

331 **Aldo F. Abarca-Ortega:** Methodology, Investigation, Writing - Review & Editing,
332 Supervision.

333 **Antonio G. Checa:** Methodology, Resources, Writing - Review & Editing, Supervision,
334 Funding acquisition.

336 **Declaration of competing interest**

337 The authors declare that they have no known competing financial interests or personal
338 relationships that could have appeared to influence the work reported in this paper.

References

- [1] Nelson Valdivia and Martin Thiel. Effects of point-source nutrient addition and mussel removal on epibiotic assemblages in perumytilus purpuratus beds. *Journal of Sea Research*, 56(4):271–283, 2006. ISSN 1385-1101. doi: <https://doi.org/10.1016/j.seares.2006.06.003>. URL <https://www.sciencedirect.com/science/article/pii/S1385110106000864>.
- [2] Jorge L. Alvarado and Juan C. Castilla. *Tridimensional matrices of mussels Perumytilus purpuratus on intertidal platforms with varying wave forces in central Chile*, volume 133. Marine Ecology Progress Series, 1996. doi: 10.3354/meps133135.
- [3] Guiñez. *Dinámica poblacional del chorito maico, Perumytilus purpuratus (Lamarck, 1819) (Bivalvia: Mytilidae), en gradientes de exposición al oleaje*. PhD thesis, Pontificia Universidad Católica de Chile, 1996.
- [4] Luis Prado and Juan Carlos Castilla. The bioengineer perumytilus purpuratus (mollusca: Bivalvia) in central chile: biodiversity, habitat structural complexity and environmental heterogeneity. *Journal of the Marine Biological Association of the United Kingdom*, 86(2):417–421, 2006. doi: 10.1017/S0025315406013282.
- [5] Brendan P. Kelaher, Juan Carlos Castilla, and Luis Prado. Is there redundancy in bioengineering for molluscan assemblages on the rocky shores of central chile? *Revista Chilena de Historia Natural*, 80(2):173–186, 2007. ISSN 07176317. doi: 10.4067/S0716-078X2007000200004.
- [6] D A Lopez, M L Gonzalez, M V Vial, and R W Simpfendorfer. Sublethal effects provoked by the presence of the predator *Nucella crassilabrum* (lamarck) upon the mussel *Perumytilus purpuratus* (lamarck) in chile. *Revista Chilena De Historia Natural*, 68(4):469–475, 1995. ISSN 0716-078X.
- [7] S. Gordillo. Predation signs by acanthina fischer von waldheim, 1807 (gasteropoda: Muricidae) on bivalvia. *Ameghiniana*, 38(1):55–60, 2001.
- [8] Sergio A. Navarrete and Juan C. Castilla. Experimental determination of predation intensity in an intertidal predator guild: dominant versus subordinate prey. *Oikos*, 100(2):251–262, 2003. doi: <https://doi.org/10.1034/j.1600-0706.2003.11996.x>. URL <https://onlinelibrary.wiley.com/doi/abs/10.1034/j.1600-0706.2003.11996.x>.
- [9] Evie A. Wieters, Steven D. Gaines, Sergio A. Navarrete, Carol A. Blanchette, and Bruce A. Menge. Scales of dispersal and the biogeography of marine predator-prey interactions. *The American Naturalist*, 171(3):405–417, 2008. doi: 10.1086/527492. URL <https://doi.org/10.1086/527492>. PMID: 18220482.
- [10] Patricio H. Manríquez, María Elisa Jara, Tania Opitz, Juan Carlos Castilla, and Nelson A. Lagos. Effects of predation risk on survival, behaviour and morphological traits of small juveniles of concholepas (loco). *Marine Ecology Progress Series*, 472:169–183, 2013. ISSN 01718630. doi: 10.3354/meps10055.
- [11] Patricio H. Manríquez, María Elisa Jara, María Loreto Mardones, Rodrigo Torres, Jorge M. Navarro, Marco A. Lardies, Cristian A. Vargas, Cristián Duarte, and Nelson A. Lagos. Ocean acidification affects predator avoidance behaviour but not prey detection in the early ontogeny of a keystone species. *Marine Ecology Progress Series*, 502:157–167, 2014. ISSN 01718630. doi: 10.3354/meps10703.
- [12] Patricio H. Manríquez, Claudio P. González, Mylene Seguel, M. Roberto Garcia-Huidobro, Karin B. Lohrmann, Paolo Domenici, Sue-Ann Watson, Cristián Duarte, and Katherine Brokordt. The combined effects of ocean acidification and warming on a habitat-forming shell-crushing predatory crab. *Science of The Total Environment*, 758:143587, 2021. ISSN 0048-9697. doi: <https://doi.org/10.1016/j.scitotenv.2020.143587>. URL <https://www.sciencedirect.com/science/article/pii/S0048969720371187>.
- [13] Jesús Acevedo, Fernanda I. Orellana, and Ricardo Guiñez. Evaluación experimental de la toxicidad de cobre in situ sobre la fauna asociada a perumytilus purpuratus (bivalvia: Mytilidae), un ingeniero ecosistémico. *Revista de Biología Marina y Oceanografía*, 45(3):497–505, 2010. ISSN 07181957. doi: 10.4067/S0718-19572010000300014.
- [14] Claudia A. Pérez, Nelson A. Lagos, Gonzalo S. Saldías, George Waldbusser, and Cristian A. Vargas. Riverine discharges impact physiological traits and carbon sources for shell carbonate in the marine intertidal mussel perumytilus purpuratus. *Limnology and Oceanography*, 61(3):969–983, 2016.

- doi: <https://doi.org/10.1002/lno.10265>. URL <https://aslopubs.onlinelibrary.wiley.com/doi/abs/10.1002/lno.10265>.
- [15] Laura Ramajo, Núria Marbà, Luis Prado, Sophie Peron, Marco A. Lardies, Alejandro B. Rodriguez-Navarro, Cristian A. Vargas, Nelson A. Lagos, and Carlos M. Duarte. Biomineralization changes with food supply confer juvenile scallops (*Argopecten purpuratus*) resistance to ocean acidification. *Global Change Biology*, 22(6):2025–2037, 2016. doi: <https://doi.org/10.1111/gcb.13179>. URL <https://onlinelibrary.wiley.com/doi/abs/10.1111/gcb.13179>.
- [16] Marco A. Lardies, Samanta Benitez, Sebastian Osores, Cristian A. Vargas, Cristián Duarte, Karin B. Lohrmann, and Nelson A. Lagos. Physiological and histopathological impacts of increased carbon dioxide and temperature on the scallops *Argopecten purpuratus* cultured under upwelling influences in northern chile. *Aquaculture*, 479:455–466, 2017. ISSN 0044-8486. doi: <https://doi.org/10.1016/j.aquaculture.2017.06.008>. URL <https://www.sciencedirect.com/science/article/pii/S0044848616312996>.
- [17] Luisa M. Saavedra, Diego Parra, Valeska San Martin, Nelson A. Lagos, and Cristian A. Vargas. Local habitat influences on feeding and respiration of the intertidal mussels *Perumytilus purpuratus* exposed to increased pCO₂ levels. *Estuaries and Coasts*, 41(4):1118–1129, 2018. ISSN 15592731. doi: 10.1007/s12237-017-0333-z.
- [18] Pablo A. Oyarzún, Jorge E. Toro, José Garcés-Vargas, Claudia Alvarado, Ricardo Guiñez, Roberto Jaramillo, Carolina Briones, and Bernardita Campos. Reproductive patterns of mussel *Perumytilus purpuratus* (bivalvia: Mytilidae), along the chilean coast: Effects caused by climate change? *Journal of the Marine Biological Association of the United Kingdom*, 98(2):375–385, 2018. ISSN 14697769. doi: 10.1017/S0025315416001223.
- [19] Joan A. Kleypas. *CHAPTER FOURTEEN: Impacts of Ocean Acidification on Marine Biodiversity*, pages 193–203. Yale University Press, 2019. doi: doi:10.12987/9780300241198-022. URL <https://doi.org/10.12987/9780300241198-022>.
- [20] Laura Ramajo, Luis Prado, Alejandro B. Rodriguez-Navarro, Marco A. Lardies, Carlos M. Duarte, and Nelson A. Lagos. Plasticity and trade-offs in physiological traits of intertidal mussels subjected to freshwater-induced environmental variation. *Marine Ecology Progress Series*, 553:93–109, 2016. ISSN 01718630. doi: 10.3354/meps11764.
- [21] J.D. Taylor and M. Layman. The mechanical properties of bivalve (mollusca) shell structure. *Paleontology*, 15(7):73–87, 1972.
- [22] Antonio G. Checa. Physical and biological determinants of the fabrication of molluscan shell microstructures. *Frontiers in Marine Science*, 5:353, 2018. ISSN 2296-7745. doi: 10.3389/fmars.2018.00353. URL <https://www.frontiersin.org/article/10.3389/fmars.2018.00353>.
- [23] Ulrike G.K. Wegst, Hao Bai, Eduardo Saiz, Antoni P. Tomsia, and Robert O. Ritchie. Bioinspired structural materials. *Nature Materials*, 14(1):23–36, 2015. ISSN 14764660. doi: 10.1038/nmat4089.
- [24] Jiyu Sun and Bharat Bhushan. Hierarchical structure and mechanical properties of nacre: a review. *RSC Adv.*, 2:7617–7632, 2012. doi: 10.1039/C2RA20218B. URL <http://dx.doi.org/10.1039/C2RA20218B>.
- [25] Marc André Meyers, Albert Yu-Min Lin, Po-Yu Chen, and Julie Muyco. Mechanical strength of abalone nacre: Role of the soft organic layer. *Journal of the Mechanical Behavior of Biomedical Materials*, 1(1):76–85, 2008. ISSN 1751-6161. doi: <https://doi.org/10.1016/j.jmbbm.2007.03.001>. URL <https://www.sciencedirect.com/science/article/pii/S1751616107000021>.
- [26] François Barthelat, Chun Ming Li, Claudia Comi, and Horacio D. Espinosa. Mechanical properties of nacre constituents and their impact on mechanical performance. *Journal of Materials Research*, 21(8):1977–1986, 2006. ISSN 08842914. doi: 10.1557/jmr.2006.0239.
- [27] Marc André Meyers, Po-Yu Chen, Albert Yu-Min Lin, and Yasuaki Seki. Biological materials: Structure and mechanical properties. *Progress in Materials Science*, 53(1):1–206, 2008. ISSN 0079-6425. doi: <https://doi.org/10.1016/j.pmatsci.2007.05.002>. URL <https://www.sciencedirect.com/science/article/pii/S0079642507000254>.
- [28] Francois Barthelat and Deju Zhu. A novel biomimetic material duplicating the structure and mechanics of natural nacre. *Journal of Materials Research*, 26(10):1203–1215, 2011. ISSN 08842914. doi: 10.1557/jmr.2011.65.

- [29] Mostafa Yourdkhani, Damiano Pasini, and Francois Barthelat. Multiscale mechanics and optimization of gastropod shells. *Journal of Bionic Engineering*, 8(4):357–368, 2011. ISSN 16726529. doi: 10.1016/S1672-6529(11)60041-3. URL [http://dx.doi.org/10.1016/S1672-6529\(11\)60041-3](http://dx.doi.org/10.1016/S1672-6529(11)60041-3).
- [30] Francois Barthelat. Nacre from mollusk shells: a model for high-performance structural materials. *Bioinspiration & Biomimetics*, 5(3):035001, aug 2010. doi: 10.1088/1748-3182/5/3/035001. URL <https://doi.org/10.1088/1748-3182/5/3/035001>.
- [31] Marc A. Meyers, Po-Yu Chen, Maria I. Lopez, Yasuaki Seki, and Albert Y.M. Lin. Biological materials: A materials science approach. *Journal of the Mechanical Behavior of Biomedical Materials*, 4(5):626–657, 2011. ISSN 1751-6161. doi: <https://doi.org/10.1016/j.jmbbm.2010.08.005>. URL <https://www.sciencedirect.com/science/article/pii/S1751616110001128>. Special Issue on Natural Materials / Papers from the Third International Conference on the Mechanics of Biomaterials and Tissues.
- [32] Larry A. Taber. Biomechanics of growth, remodeling, and morphogenesis. *Applied Mechanics Reviews*, 48(8):487–545, 1995. ISSN 00036900. doi: 10.1115/1.3005109. URL <https://doi.org/10.1115/1.3005109>.
- [33] F. Barthelat, J.E. Rim, and H.D. Espinosa. *A Review on the Structure and Mechanical Properties of Mollusk Shells - Perspectives on Synthetic Biomimetic Materials*, pages 17–44. Springer Berlin Heidelberg, Berlin, Heidelberg, 2009. ISBN 978-3-540-85049-6. doi: 10.1007/978-3-540-85049-6_2. URL https://doi.org/10.1007/978-3-540-85049-6_2.
- [34] F. Song and Y. L. Bai. Effects of nanostructures on the fracture strength of the interfaces in nacre. *Journal of Materials Research*, 18(8):1741–1744, 2003. ISSN 08842914. doi: 10.1557/JMR.2003.0239.
- [35] Guowei Chen, Hongyun Luo, Shunfei Luo, Zhenying Lin, and Yue Ma. Vertically oriented structure and its fracture behavior of the indonesia white-pearl oyster. *Journal of the Mechanical Behavior of Biomedical Materials*, 66:211–223, 2017. ISSN 1751-6161. doi: <https://doi.org/10.1016/j.jmbbm.2016.11.002>. URL <https://www.sciencedirect.com/science/article/pii/S1751616116303794>.
- [36] Jingru Song, Cuncai Fan, Hansong Ma, Lihong Liang, and Yueguang Wei. Crack deflection occurs by constrained microcracking in nacre. *Acta Mechanica Sinica/Lixue Xuebao*, 34(1):143–150, 2018. ISSN 16143116. doi: 10.1007/s10409-017-0724-1.
- [37] Madeleine Grossman, Florian Bouville, Kunal Masania, and André R. Studart. Quantifying the role of mineral bridges on the fracture resistance of nacre-like composites. *Proceedings of the National Academy of Sciences*, 115(50):12698–12703, 2018. ISSN 0027-8424. doi: 10.1073/pnas.1805094115. URL <https://www.pnas.org/content/115/50/12698>.
- [38] Najmul Abid, J William Pro, and Francois Barthelat. Fracture mechanics of nacre-like materials using discrete-element models: Effects of microstructure, interfaces and randomness. *Journal of the Mechanics and Physics of Solids*, 124:350–365, 2019. ISSN 0022-5096. doi: <https://doi.org/10.1016/j.jmps.2018.10.012>. URL <https://www.sciencedirect.com/science/article/pii/S0022509618303430>.
- [39] Ryan P. Wilkerson, Bernd Gludovatz, Jeremy Watts, Antoni P. Tomsia, Gregory E. Hilmas, and Robert O. Ritchie. A novel approach to developing biomimetic (“nacre-like”) metal-compliant-phase (nickel-alumina) ceramics through coextrusion. *Advanced Materials*, 28(45):10061–10067, 2016. doi: <https://doi.org/10.1002/adma.201602471>. URL <https://onlinelibrary.wiley.com/doi/abs/10.1002/adma.201602471>.
- [40] Bedabibhas Mohanty, Kalpana S. Katti, Dinesh R. Katti, and Devendra Verma. Dynamic nanomechanical response of nacre. *Journal of Materials Research*, 21(8):2045–2051, 2006. ISSN 08842914. doi: 10.1557/jmr.2006.0247.
- [41] Jiddu Bezares, Zhangli Peng, Robert Asaro, and Qiang Zhu. Macromolecular structure and viscoelastic response of the organic framework of nacre in haliotis rufescens: A perspective and overview. *Theoretical and Applied Mechanics Teorijska i primenjena mehanika*, 38(2):75–106, 2011. ISSN 1450-5584. doi: 10.2298/tam1102075b.
- [42] Françoise Immel, Cédric Broussard, Bastien Catherinet, Laurent Plasseraud, Gérard Alcaraz, Irina Bundeleva, and Frédéric Marin. The shell of the invasive bivalve species dreissena polymorpha: Biochemical, elemental and textural investigations. *PLOS ONE*, 11(5):1–28, 05 2016. doi: 10.1371/journal.pone.0154264. URL <https://doi.org/10.1371/journal.pone.0154264>.
- [43] Clara L. Mackenzie, Graham A. Ormondroyd, Simon F. Curling, Richard J. Ball, Nia M. Whiteley, and

- Shelagh K. Malham. Ocean warming, more than acidification, reduces shell strength in a commercial shellfish species during food limitation. *PLOS ONE*, 9(1):1–9, 01 2014. doi: 10.1371/journal.pone.0086764. URL <https://doi.org/10.1371/journal.pone.0086764>.
- [44] Wen Yang, Neima Kashani, Xiao-Wu Li, Guang-Ping Zhang, and Marc André Meyers. Structural characterization and mechanical behavior of a bivalve shell (*saxidomus purpuratus*). *Materials Science and Engineering: C*, 31(4):724–729, 2011. ISSN 0928-4931. doi: <https://doi.org/10.1016/j.msec.2010.10.003>. URL <https://www.sciencedirect.com/science/article/pii/S0928493110002407>. Sixth Symposium on Biological Materials Science, 139th Annual Meeting & Exhibition of The Minerals, Metals & Materials Society.
- [45] D. Jiao, Z.Q. Liu, Y.K. Zhu, Z.Y. Weng, and Z.F. Zhang. Mechanical behavior of mother-of-pearl and pearl with flat and spherical laminations. *Materials Science and Engineering: C*, 68:9–17, 2016. ISSN 0928-4931. doi: <https://doi.org/10.1016/j.msec.2016.05.089>. URL <https://www.sciencedirect.com/science/article/pii/S0928493116305227>.
- [46] Susan C. Fitzer, Wenzhong Zhu, K. Elizabeth Tanner, Vernon R. Phoenix, Nicholas A. Kamenos, and Maggie Cusack. Ocean acidification alters the material properties of *Mytilus edulis* shells. *Journal of The Royal Society Interface*, 12(103):20141227, 2015. doi: 10.1098/rsif.2014.1227. URL <https://royalsocietypublishing.org/doi/abs/10.1098/rsif.2014.1227>.
- [47] Pablo Oyarzún Cabañas, Jorge E Toro, Roberto Jaramillo, Ricardo Guiñez, and Carolina Briones. Análisis comparativo del ciclo gametogénico de perumytilus purpuratus (bivalvia : Mytilidae), en las localidades de taltal y huasco , norte de chile introducción material y métodos. *Revista de biología marina y oceanografía*, 45(1):43–58, 2010.
- [48] LOZADA E; REYES P. Reproductive biology of a population of perumytilus purpuratus at el tabo, chile (mollusca: Bivalvia: Mytilidae). *VELIGER*; ISSN 0042-3211; USA; DA. 1981; VOL. 24; NO 2; PP. 147-154; H.T. 2; BIBL. 25 REF., 1981. URL <https://pascal-francis.inist.fr/vibad/index.php?action=getRecordDetail&idt=PASCALZOOLINEINRA82X0057588>.
- [49] R. Menig, M.H. Meyers, M.A. Meyers, and K.S. Vecchio. Quasi-static and dynamic mechanical response of *haliotis rufescens* (abalone) shells. *Acta Materialia*, 48(9):2383–2398, 2000. ISSN 1359-6454. doi: [https://doi.org/10.1016/S1359-6454\(99\)00443-7](https://doi.org/10.1016/S1359-6454(99)00443-7). URL <https://www.sciencedirect.com/science/article/pii/S1359645499004437>.
- [50] Mehmet Sarikaya. An introduction to biomimetics: A structural viewpoint. *Microscopy Research and Technique*, 27(5):360–375, 1994. doi: <https://doi.org/10.1002/jemt.1070270503>. URL <https://analyticalsciencejournals.onlinelibrary.wiley.com/doi/abs/10.1002/jemt.1070270503>.
- [51] Da Jiao, Zengqian Liu, Zhenjun Zhang, and Zhefeng Zhang. Intrinsic hierarchical structural imperfections in a natural ceramic of bivalve shell with distinctly graded properties. *Scientific Reports*, 5(June): 1–13, 2015. ISSN 20452322. doi: 10.1038/srep12418. URL <http://dx.doi.org/10.1038/srep12418>.
- [52] Ling Li, James C. Weaver, and Christine Ortiz. Hierarchical structural design for fracture resistance in the shell of the pteropod *clio pyramidata*. *Nature Communications*, 6:6216, 2015. ISSN 20411723. doi: 10.1038/ncomms7216. URL <https://doi.org/10.1038/ncomms7216>.
- [53] Quan Yuan, Botao Chen, Bin Chen, and Zeyun Wang. New insight into the toughening mechanisms of seashell: From arch shape to multilayer structure. *Journal of Nanomaterials*, 2016, 2016. ISSN 16874129. doi: 10.1155/2016/3817985.
- [54] R. Z. Wang, Z. Suo, A. G. Evans, N. Yao, and I. A. Aksay. Deformation mechanisms in nacre. *Journal of Materials Research*, 16(9):2485–2493, 2001. doi: 10.1557/JMR.2001.0340.
- [55] M DHANASEKAR, AW PAGE, and PW KLEEMAN. The failure of brick masonry under biaxial stresses. *Proceedings of the Institution of Civil Engineers*, 79(2):295–313, 1985. doi: 10.1680/iicep.1985.992. URL <https://doi.org/10.1680/iicep.1985.992>.
- [56] Bibiana Lucioni and Viviana C. Rougier. In-plane retrofitting of masonry panels with fibre reinforced composite materials. *Construction and Building Materials*, 25(4):1772–1788, 2011. ISSN 0950-0618. doi: <https://doi.org/10.1016/j.conbuildmat.2010.11.088>. URL <https://www.sciencedirect.com/science/article/pii/S0950061810006185>.
- [57] Vadim I. Lishak, Vladimir I. Yagust, and David Z. Yankelevsky. 2-d orthotropic failure criteria for

- masonry. *Engineering Structures*, 36:360–371, 2012. ISSN 0141-0296. doi: <https://doi.org/10.1016/j.engstruct.2011.11.033>. URL <https://www.sciencedirect.com/science/article/pii/S0141029611004809>.
- [58] Antonio Maria D’Altri, Vasilis Sarhosis, Gabriele Milani, Jan Rots, Serena Cattari, Sergio Lagomarsino, Elio Sacco, Antonio Tralli, Giovanni Castellazzi, and Stefano de Miranda. *Modeling Strategies for the Computational Analysis of Unreinforced Masonry Structures: Review and Classification*, volume 27. Springer Netherlands, 2020. ISBN 0123456789. doi: 10.1007/s11831-019-09351-x. URL <https://doi.org/10.1007/s11831-019-09351-x>.
- [59] J.A. Thamboo and M. Dhanasekar. Nonlinear finite element modelling of high bond thin-layer mortared concrete masonry. *International Journal of Masonry Research and Innovation*, 1(1):5–26, 2016. doi: 10.1504/IJMRI.2016.074727. URL <https://www.inderscienceonline.com/doi/abs/10.1504/IJMRI.2016.074727>.
- [60] M.A. Meyers, C.T. Lim, A. Li, B.R. Hairul Nizam, E.P.S. Tan, Y. Seki, and J. McKittrick. The role of organic intertile layer in abalone nacre. *Materials Science and Engineering: C*, 29(8):2398–2410, 2009. ISSN 0928-4931. doi: <https://doi.org/10.1016/j.msec.2009.07.005>. URL <https://www.sciencedirect.com/science/article/pii/S0928493109001957>.